Semiconductor Physics, Quantum Electronics & Optoelectronics. 2001. V. 4, N 4. P. 249-252.

PACS: 68.55.L; 77.84.B

Study of postimplantation annealing of SiC

S.F. Avramenko, V.S. Kiselev
Special Bureau for Design and Technology with Pilot Production Department of the Institute of Semiconductor Physics, NAS of Ukraine, 4 Lysogorskaya St., Kyiv, 03028, Ukraine
Fax: (380-44) 265-19-57; E-mail: kisvs@yandex.ru

B.N. Romanyuk, M.Ya. Valakh
Institute of Semiconductor Physics, NAS Ukraine, 45 Prospect Nauki, Kyiv, 03028, Ukraine
Tel.: (380-44) 265-61-82; Fax: (380-44) 265-83-42; E-mail: valakh@semicond.kiev.ua

Abstract. The implanted layer resistance $R/\Box$ thermoelectromotive force, optical transmittance T and open-circuit photovoltage measurements were made on epitaxial n-type 6H-SiC samples and Lely-grown 6H-SiC crystals implanted at 30° and 500 °C with Al ions annealed at 1600 to 2000 °C. The objective was to study processes of defect annealing and activation of implanted aluminum to determine the optimal parameters of the postimplantation annealing mode. It is shown that processes of radiation defect annealing and implanted aluminum activation are characterized by essentially different times that depend on the annealing and implantation conditions. Measurements of the open-circuit photovoltage U enable one to check the aluminum activation process and optimize the annealing conditions.

Keywords: silicon carbide, implantation, annealing.

Paper received 26.07.01; revised manuscript received 17.10.01; accepted for publication 12.12.01.

1. Introduction

Selective doping of crystals is required for manufacturing SiC-based semiconductor devices using planar technology. To this end, ion implantation is the most convenient. It provides local doping even with those impurities, diffusion coefficients of which are small. However, ion implantation leads to disruption of the crystal lattice in semiconductors: point defects, clusters, changes in lattice parameters, etc. At high implantation doses, a phase transition from a crystal state to the amorphous one can occur. The amorphization threshold for Al ion implantation into 6H-SiC is about 8×10^{14} cm^{-2} [1, 2]. Besides, the implanted impurity ions predominantly occupy the interstitials of the host crystal and are electrically inactive. That is why postimplantation annealing is used for crystal structure restoration, annealing of radiation defects and impurity activation. On annealing amorphous SiC layers, the polytype inclusions can appear; these polytypes may differ from those of the initial crystal. The inclusions of cubic SiC are a most often observed in implanted layers after annealing [3, 4].

The following techniques are used for annealing:
(i) thermal annealing at temperatures 1600–1800 °C (duration from 10 min. up to several hours);
(ii) flash annealing (duration of 10–30 ms);
(iii) pulse laser annealing (pulse duration of 10–20 ms).
Clearly the excess duration of high-temperature annealing could distort the doping profile due to diffusion, while deficient duration could result in only partial aluminum activation. Therefore our objective was to study processes of defect annealing and activation of implanted aluminum to determine optimal parameters of the postimplantation annealing mode.

2. Experimental

We used the samples of two types: Lely-grown 6H-SiC crystals ($N_D - N_A \approx 7\times10^{17}$ cm^{-3}) and 6H-SiC epitaxial structures ($N_D - N_A \approx 1\times10^{16}$ cm^{-3} in the epitaxial layer). All samples have been cut into plates measured 5×5 mm^2. To obtain a step *p-n* junction with uniform Al distribution, we have calculated the required energies and doses with the TRIM program. We used ions of energies 75, 125 and 180 keV; the total dose was 5.5×10^{15} cm^{-2}. Three sets of experiments

© 2001, Institute of Semiconductor Physics, National Academy of Sciences of Ukraine

have been performed. In two of them the Lely-grown crystals (L) and epitaxial structures (E) were implanted at the temperature T_i = 30 °C. In the third set only the epitaxial structures (C) implanted at T_i = 500 °C were studied.

Two setups were used to perform annealing. Rapid annealing was made with a strip heater. It enabled us to perform thermal annealing with heating rate up to 1500 °C/s and minimal annealing stage duration of 5 s. Thermal annealing was performed in the He flow. These conditions completely ruled out the possibility for epitaxial film formation on the crystal surfaces. However, at temperatures over 1900 °C and annealing duration over 30 s, the silicon carbide evaporation/dissociation from the crystal surfaces occurred. The annealing temperature T_{ann} varied from 1600 up to 2100 °C; it was monitored with an optical pyrometer.

Long-term annealing was made in Ar atmosphere at a pressure of (0.9–1.0)×10^5 Pa in a vacuum oven REDMET-30. The maximal heating rate was 50–100 °C/min. The crystals were put into a graphite crucible previously laden with silicon and silicon carbide. This eliminated the possibility of SiC dissociation. On occasion, however, we observed formation of thin epitaxial layers on the crystal end surfaces. The crucible temperature was checked with the optical pyrometer.

We characterized the crystals after each annealing. The implanted layer resistance $R/\square$, thermoelectromotive force and its sign, open-circuit photovoltage were measured with the four-probe technique. We also measured optical transmittance T. At photoelectric measurements, we used focused emission from a mercury-discharge lamp PRK-4 (power of 220 W). In addition, we checked for occurrence of electroluminescence using a photomultiplier FEU-30. To measure photoelectric properties and electroluminescence, we have deposited rectifying contacts onto the crystals on the n-region side. A tungsten needle served as contact to the implanted layer. When the optimal mode has been chosen, then we made the check one-stage annealing of several samples.

Shown in Fig. 1 are typical dependencies of the optical transmittance T on the time of annealing t_{ann} at a wavelength 650 nm. Fig. 2 presents the surface resistance of the implanted layer $R/\square$ as function of the time of annealing t_{ann}. We have not managed to perform the corresponding measurements for samples of the set C at the initial stages of annealing due to their high resistance. It was possible to make such measurements at the final stage of annealing only.

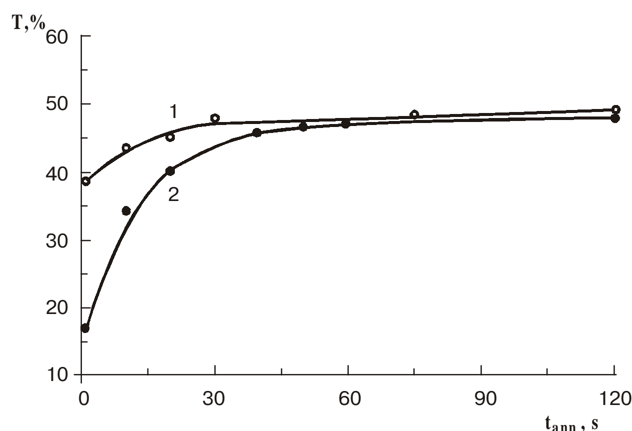

Fig. 1. The transmittance T vs time of annealing t_{ann} curves for epitaxial structures. Samples: 1 – C11 (T_{ann} = 1900 °C); 2 – E11 (T_{ann} = 1700 °C).

Shown in Fig. 3 is the open-circuit photovoltage U as a function of the time of annealing t_{ann}. The Table 1 gives the experimental values and results of graphical display processing for the samples of sets E and C.

3. Discussion of results

In models used for analysis of mechanisms for radiation defect annealing [5] the time of annealing enters into the theoretical expressions through the ratio t/τ where τ is the average time required for transfer of an atom from a position in the crystal lattice to another position. The τ value depends on the temperature and energy of vacancy migration. From an analysis of the experimental data it follows that they could be adequately described by exponentials with two characteristic times that correspond to the follow-

Table 1. Experimental values of the open-circuit photovoltage U and implanted layer resistance $R/\square$, as well as photovoltage characteristic time τ_{ph} calculated from the experimental plots. (d is the number of annealing stages; t_Σ is the total annealing duration.)

Sample #	T_i, °C	T_{ann}, °C	U, V	τ_{ph}, s	$R/\square$, 10^4 Ω	Comments
E11	30	1700	1.2		1	multistage annealing, d = 11, t_Σ = 23 min.
E19	30	1820			2.5	multistage annealing, d = 6, t_Σ = 1.5 min.
E4	30	1900	1.4	80	3.5	multistage annealing, d = 13, t_Σ = 8 min.
E20	30	2000			4.5	one-stage annealing for 2.5 min; partial evaporation of the implanted layer
C10	500	1700	1.80	75	1	multistage annealing, d = 8, t_Σ = 22 min.
C12	500	1800	2.15	70	3.2	multistage annealing, d = 24, t_Σ = 19 min.
C11	500	1900	2.20	66	1.3	multistage annealing, d = 21, t_Σ = 15 min.
C13	500	2000	2.17	35	3.7	multistage annealing, d = 13, t_Σ = 5.5 min.
C14	500	1800	2.14		2.2	one-stage annealing for 4.5 min.
C15	500	1865	2.15		0.87	one-stage annealing for 5 min.

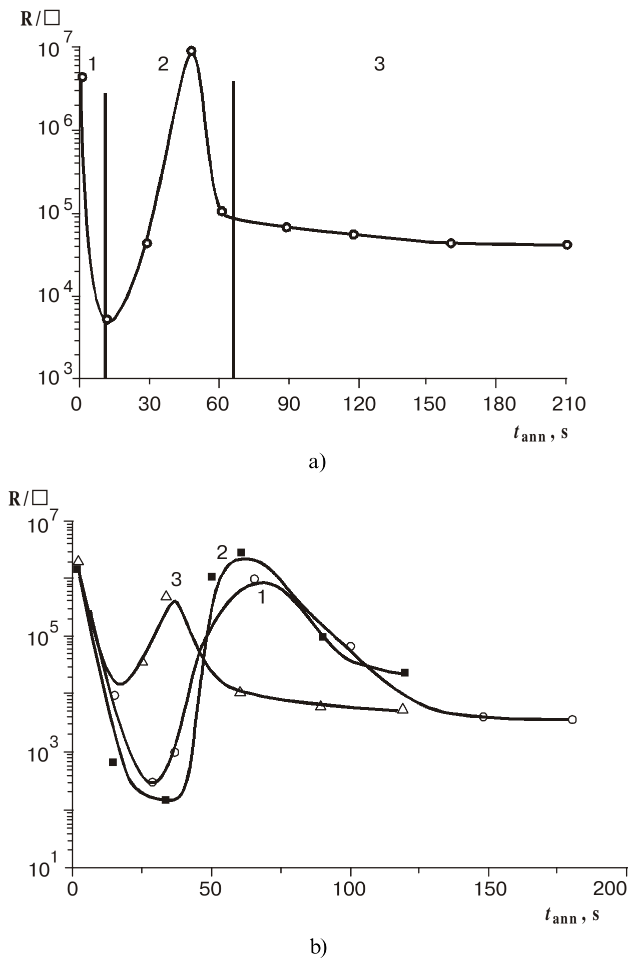

Fig. 2. The implanted layer resistance $R/\square$ vs time of annealing t_{ann} curves: *a* – sample E11 (T_{ann} = 1700 °C); *b* – Lely crystals: 1 – L25 (T_{ann} =1640 °C), 2 – L26 (T_{ann} =1740 °C), 3 – L27 (T_{ann} =1835 °C).

ing physical processes: annealing of radiation defects and activation of aluminum ions.

Optical transmittance. One can see from Fig. 1 that annealing leads to an increase of crystal transparency. This results from the restoration of crystal structure. The above process of transmittance increasing could be adequately described by the following expression:

$$T = T_1 + (T_0 - T_1)[1 - \exp(-t/\tau_{opt})].$$

Here T_1 is the crystal transmittance before annealing; T_0 is the transmittance of the completely annealed crystal; t_{opt} is the characteristic time (it equals to 12–15 s). One can see that, as one would expect, in the initial state the optical transmittance is considerably higher for the epitaxial structures implanted at a temperature of 500 °C (set C0 than for the samples implanted at 30 °C (set E).

Surface resistance. One can see from Fig. 2 that the implanted layer resistance $R/\square$ vs time of annealing t_{ann} curves have three distinguishing stages. At first the resistance rapidly goes down. This process (similarly to that of the optical transmittance growth that was mentioned above) can be described as an exponential with a characteristic time. This time closely agrees with t_{opt}. So one can draw a logical deduction that it is the crystal structure restoration that serves as predominant physical reason for resistance changing at this stage.

At the second stage the conduction type is conversed from *n*- to *p*-type due to impurity activation. Accordingly a peak appears on the $R/\square = f(t_{ann})$ curve. The time dependence of resistance at this stage can be expressed as

$$R/\square \approx \{e\mu_n n - e\mu_p p[1 - \exp(-t/\tau_R)]\}^{-1}.$$

Here e is the elementary charge; n and μ_n (p and μ_p) are the electron (hole) concentration and mobility, respectively; τ_R is time that characterizes the process of activation of implanted acceptor centers. It is evident that concentration of electrically active aluminum centers grows with implantation dose, and at some moment the inversion of conductivity occurs. The peak position depends on the annealing temperature: when T_{ann} grows, then the peak shifts toward smaller t_{ann} values.

At the third stage the resistance $R/\square$ is slowly decreasing due to continuing aluminum activation. A slope of the corresponding curve on the plot is small, so it is difficult to estimate the optimal duration of annealing. One can see from Table 1 that at rather big values of t_{ann} and high temperatures $R/\square \leq 1\times10^4\,\Omega$; this corresponds to the average concentration $p = 5\times10^{18}$ cm^{-3}

Photoeffect. Considerable photovoltaic effect was observed in all the epitaxial structures studied. Activation of aluminum ions during annealing leads to appearance of *p*-region and formation of *p-n* junction. The equilibrium charge carrier concentration in the *p*-region increases with time of annealing; as a result, the potential barrier of the *p-n* junction becomes higher. In [6] it was shown that at high illumination level the maximal value of open-circuit photovoltage is proportional to the above potential barrier height. Therefore one can get information on the potential barrier height and its change due to annealing from the photovoltage measurements. The photovoltage dependence on annealing duration can be presented as $U = U_m[1 - \exp(-t/\tau_{ph})]$. This expression is in good agreement with the experimental curves given in Fig. 3. It follows from them that when annealing duration is increased, then the photovoltage grows. One can see from Fig. 4 that the highest U values are observed at annealing temperatures $T_{ann} \geq 1850$ °C.

Electroluminescence. Table 1 gives the data on electroluminescence. It should be noted that no luminescence was observed for the Lely crystals (set L). For some samples of set C we have registered luminescence in the blue spectral region. Most of the samples belonging to sets E and C demonstrated luminescence in the green spectral region. We believe that electroluminescence cannot serve as criterion for aluminum activation, because it is observed even at early stages of annealing, and we have not detected considerable dependence of the luminescence intensity on the annealing duration.

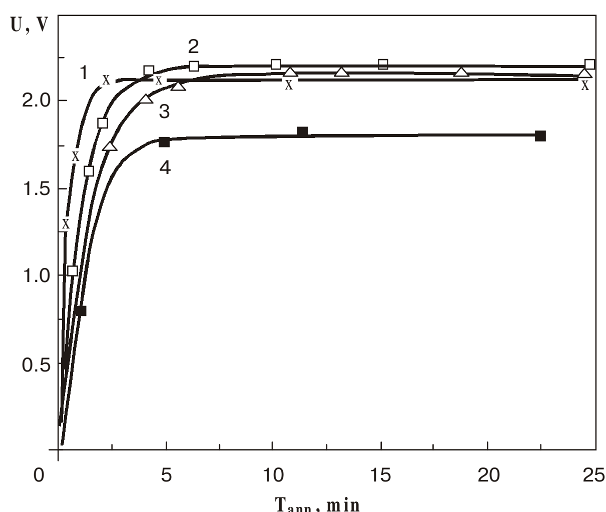

Fig. 3. The open-circuit photovoltage U vs time of annealing t_{ann} curves. Dots – experimental results for the samples: 1 – C13 (T_{ann} = 2000 °C), 2 – C11 (T_{ann} = 1900 °C), 3 – C12 (T_{ann} = 1800 °C), 4 – C10 (T_{ann} = 1700 °C); full curves give the calculated dependencies $U = U_m[1 - \exp(-t/\tau_{ph})]$.

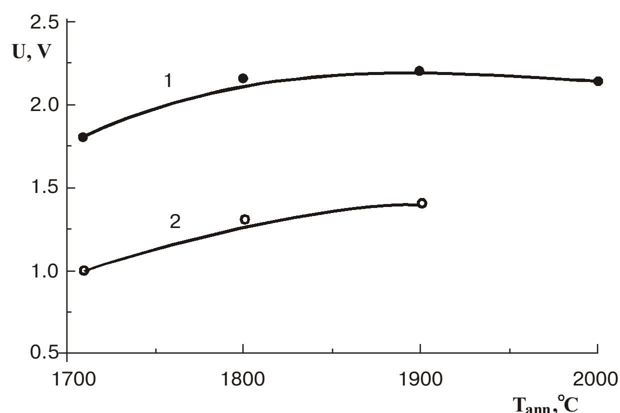

Fig. 4. The maximum open-circuit photovoltage U value vs time of annealing t_{ann} curves. Samples: 1 – of the set C (T_i = 500 °C), 2 – of the set E (T_i = 30 °C).

Conclusions

1. It is shown that processes of radiation defect annealing and implanted aluminum activation are characterized by essentially different times that depend on the annealing and implantation conditions.

2. Measurements of the open-circuit photovoltage U enable one to check the aluminum activation process and optimize the annealing conditions, based on the time at which U vs t_{ann} curves flatten out. Further increase of annealing duration does not result in substantial growth of the activation degree for the implanted aluminum. In our case the optimal annealing temperature was $T_{ann} \geq 1850$ °C. Clearly growth of annealing temperature favors further activation of aluminum ions; however, at higher temperatures we could not manage to circumvent processes leading to surface quality deterioration.

3. The impurity activation essentially depends on the implantation conditions. At low implantation temperature (set E) the photovoltage is substantially below that for the samples implanted at 500 °C (set C).

References

1. N. Chechenin, K. Bourdelle, A. Suvorov, A. Kastilio-Vitloch // *Nucl. Instr. and Meth.* **B65**, p. 341 (1992).
2. A. Heft, E. Wendeler, T. Bachmann, E. Glaser, W. Wesch // *Mater. Sci. and Eng.* **B29**, pp. 142-146 (1995).
3. E.E. Violin, E.A. Gorin, E.N. Potapov, Yu.M. Tairov // *Pisma v ZhTF*, **10**(24), pp. 1527-1529 (1984) (in Russian).
4. E.E. Violin, K.D. Demakov, A.A. Kalinin, F. Neubert, E.N. Potapov, Yu.M. Tairov // *Fiz. Tverd. Tela*, **26**(5), pp. 1575-1577 (1984) (in Russian).
5. R.C. Fletcher, W.C. Brown // *Phys. Rev.*, **92**(3), pp. 585-590 (1953).
6. P.N. Keating // *J. Appl. Phys.*, **36**, pp. 569-570 (1965).